IEEE Access
Multidisciplinary | Rapid Review | Open Access Journal

Received June 16, 2021, accepted June 21, 2021, date of publication June 28, 2021, date of current version July 6, 2021.

Digital Object Identifier 10.1109/ACCESS.2021.3092827

Symmetrical Pole Placement Method-Based Unity Proportional Gain Resonant and Gain Scheduled Proportional (PR-P) Controller With Harmonic Compensator for Single Phase Grid-Connected PV Inverters

CAGFER YANARATES AND ZHONGFU ZHOU
Electrical and Electronic Engineering Department, Swansea University Bay Campus, Swansea SA1 8EN, U.K.
Corresponding author: Cagfer Yanarates (887912@swansea.ac.uk)

This work was supported in part by the European Regional Development Fund (ERDF) through the FLEXIS Project.

This work did not involve human subjects or animals in its research.

ABSTRACT In this paper, a symmetrical pole placement Method-based Unity Proportional Gain Resonant and Gain Scheduled Proportional (PR-P) Controller is presented. The proposed PR-P controller resolved the issues that are tracking repeating control input signal with zero steady-state and mitigating of 3rd order harmonic component injected into the grid associated with the use of PI controller for single-phase PV systems. Additionally, the PR-P controller has overcome the drawbacks of frequency detuning in the grid and increase in the magnitude of odd number harmonics in the system that constitute the common concerns in the implementation of conventional PR controller developed as an alternative to PI controller. Moreover, the application of an unprecedented design process based on changing notch filter dynamics with symmetrical pole placement around resonant frequency overcomes the limitations that are essentially complexity and dependency on the precisely modelled system associated with the use of various controllers such as Adaptive, Predictive and Hysteresis in grid connected PV power generation systems. The proposed PR-P controller was validated employing Photovoltaic emulator (PVE) consisting of a DC-DC Buck power converter, a maximum power point tracking (MPPT) algorithm and a full-bridge grid connected inverter designed using MATLAB/Simulink system platform. Details of the proposed controller, Photovoltaic emulator (PVE) simulations, analysis and test results were presented in the paper.

INDEX TERMS Proportional resonant current controller, harmonic compensator, buck converter based PV emulator, MPPT.

I. INTRODUCTION

Over the last two decades, energy generation has shown a great tendency to utilize the renewable sources due to the facts that depletion of the fossil fuels, increasing concern of the environmental issues, energy security, productivity growth and reduction of the overall cost of power generation-distribution systems as a result of technological developments [1], [2]. Photovoltaic (PV) energy is a clean, renewable source of direct current (DC) energy generated from the sunlight, which attracts considerable attention due to remarkable advantages such as reliability and long-life, advanced manufacturing process, static and noise-free operations, increasing efficiency, decreasing prices, flexibility of construction and availability of government support and incentives [3], [4]. The increasing demand of PV energy systems has leaded to comprehensive studies in this field, common ground of these studies aims at achieving the increase in the efficiency, reliability and useful life-span of the PV systems and on the contrary the reduction in cost and space from generation to delivering of the energy [5], [6]. Single-phase PV inverter systems have been widely applied in photovoltaic power generation. Inverter current control with the object of injecting smooth current with less harmonics

The associate editor coordinating the review of this manuscript and approving it for publication was Chi-Seng Lam.

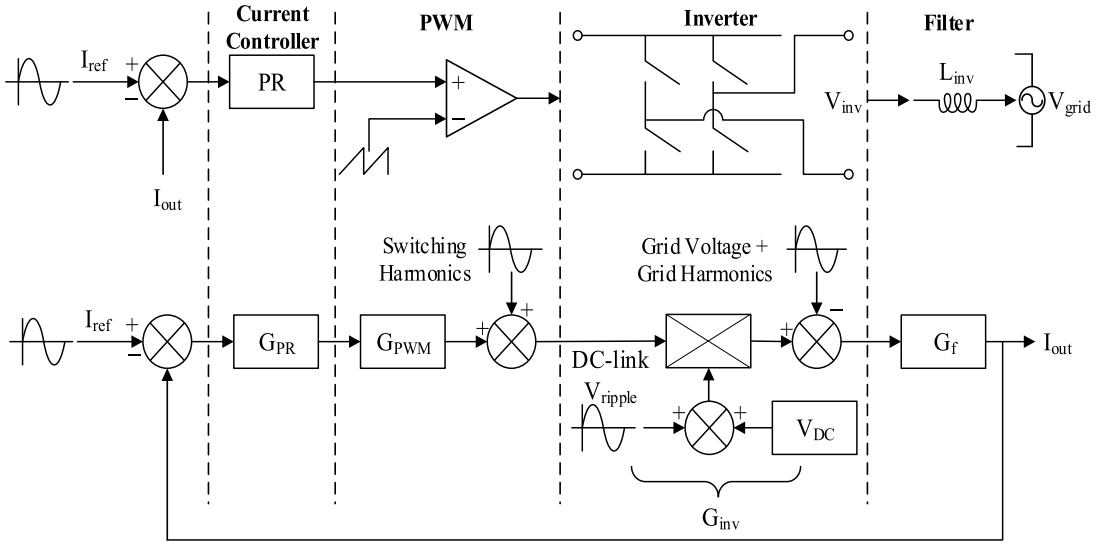

FIGURE 1. Current controlled PWM inverter with harmonic information.

to the grid is the key aspect of the PV power sourced grid connected inverter (GCI) systems [7]. The main reasons of harmonic generation in single phase PV inverter systems are basically due to distortion in the grid voltage, switching harmonics (high frequency) and DC-link voltage variations arising from the MPPT [8], [9]. The basic model of closed loop Pulse Width Modulation (PWM) current controlled single- phase inverter with harmonic information is given in Figure 1, where G_{PR}, G_{PWM}, G_{inv} and G_f are PR controller, PWM, inverter and filter transfer functions, respectively.

It is crucial to state that distortions in the current for the single-phase GCI systems are particularly caused by the PWM control of the inverter and variations in the DC-link voltage [9]. Considering that the fundamental grid voltage $v_g^1 = \sqrt{2}\, V_g^1 \cos(\omega_0 t + \varphi)$, the fundamental grid current $i_g^i = \sqrt{2}\, I_g^1 \cos(\omega_0 t)$, the inverter output voltage $v_{inv}^1 = \sqrt{2}\, V_{inv}^1 \cos(\omega_0 t + \varphi - \varphi_1)$, the DC side instantaneous power P_{dc} (i.e., PV array output power) and the instantaneous inverter output power P_{inv} for the single-phase inverter PV system can be obtained as

$$\begin{aligned} P_{dc} &= v_{pv} i_{pv} - v_{pv} C_{dc} \frac{dv_{pv}}{dt} \\ &= v_{pv} i_{pv} - V_{pv} C_{dc} \frac{d\tilde{v}_{pv}}{dt} - \tilde{v}_{pv} C_{dc} \frac{d\tilde{v}_{pv}}{dt} \end{aligned} \tag{1}$$

$$\begin{aligned} P_{inv} &= v_{inv}^1 i_g^1 \\ &= \sqrt{2} V_{inv}^1 cos\,(\omega_0 t + \varphi - \varphi_1)\, \sqrt{2} I_g^1 cos\,(\omega_0 t) \\ &= V_{inv}^1 I_g^1 cos\,(\varphi - \varphi_1) + V_{inv}^1 I_g^1 cos\,(2\omega_0 t + \varphi - \varphi_1) \\ &\quad + \left(i_g^1 \sum_{h=2}^{n} v_{inv}^h + v_{inv}^1 \sum_{h=2}^{n} i_g^h \right) \end{aligned} \tag{2}$$

where V_g^1, I_g^1, V_{inv}^1, ω_0, φ, φ_1, v_{pv}, i_{pv}, C_{dc}, V_{pv}, $\tilde{v}_{pv}$, i_g^h, v_{inv}^h represents amplitude of the fundamental grid voltage, amplitude of the fundamental grid current, amplitude of the fundamental inverter output voltage, fundamental angular frequency, power angle, inverter voltage leading angle, PV voltage, PV current, DC-link capacitance, DC component of the PV voltage, AC component of the PV voltage, grid current harmonics and inverter voltage harmonics, respectively.

For a single-phase PV system, neglecting the inverter and DC-link capacitor losses gives $P_{dc} = P_{inv}$. Ignoring the high order term $\tilde{v}_{pv} d\tilde{v}_{pv}/dt$ in the DC side instantaneous power and considering the relationships of $|V_{pv}| \gg |\tilde{v}_{pv}|$, $|I_g^1| \gg |i_g^h|$, and $|V_{inv}^1| \gg |v_{inv}^h|$, equivalence of the powers obtained in (1) and (2) yields

$$\tilde{v}_{pv} \approx -\int \left[\frac{V_{inv}^1 I_g^1}{C_{dc} V_{pv}} \cos\,(2\omega_0 t + \varphi - \varphi_1) \right] dt \tag{3}$$

which confirms that the PV source output (the DC-link voltage) pulsate at twice the grid frequency and amplitude of its variation is proportional to fundamental amplitude of the inverter output voltage V_{inv}^1 and fundamental amplitude of the grid current I_g^1.

The inverter output voltage harmonics induction is strictly dominated for the injected current in the grid, since DC-to-AC inversion is executed by the application of the PWM scheme using non-linear semiconductor devices. In general terms, the PWM current controlled single-phase inverter output voltage v_{inv} can be expressed as

$$\begin{aligned} v_{inv} &= d_{pwm} v_{pv} = \left(d_{pwm}^1 + \sum_{h=2}^{n} d_{pwm}^h \right) \left(V_{pv} + \tilde{v}_{pv} \right) \\ &= d_{pwm}^1 V_{pv} + d_{pwm}^1 \tilde{v}_{pv} + V_{pv} \sum_{h=2}^{n} d_{pwm}^h \\ &\quad + \tilde{v}_{pv} \sum_{h=2}^{n} d_{pwm}^h = v_{inv}^1 + \sum_{h=2}^{n} v_{inv}^h \end{aligned} \tag{4}$$

where d_{pwm}, d^1_{pwm}, and d^h_{pwm} are the PWM signal, fundamental component of the PWM and harmonics of the PWM, respectively. In theory, formation of the PWM harmonics $\sum_{h=2}^{n} d^h_{pwm}$ occurs around the switching frequency and its multiples that corresponds to generation of the high order harmonics [10]. However, practical applications show that the PWM harmonics contributes to low order harmonic distortions due to dead-time and non-linear ON-OFF switching [10], [11]. Eq (4) indicates that variation $\tilde{v}_{pv}$ will introduce harmonics in the inverter output voltage and it mainly contains even harmonics at the double of the grid frequency $2\omega_0$ shown in (3). The term $d^1_{pwm}\tilde{v}_{pv}$ in (4) implies that odd current harmonics injection is inevitable in single-phase PV inverter systems with the frequency of $(2k+1)\,\omega_0, k = 1, 2, 3, \ldots$ [9]. The second order harmonic on the DC side will be converted as a third-order harmonic on the grid side that is the primary problem for the single-phase PV inverter systems. The main purpose of this study is to eliminate the 3rd order harmonics in grid side that stems from 2nd order harmonic component in PV side caused by the Dc-link voltage variations due to MPPT.

According to the IEEE Std 519-1992, total harmonic distortion (THD) shall be less than 5% of the current at the fundamental frequency at rated power output of the inverter and the distortion limits of the individual harmonics shall be less than 4%, 2%, 1.5%,0.6% and 0.3% for 3rd to 9th, 11th to 15th,17th to 21st, 23rd to 33rd and the odd harmonics above 33rd, respectively [12]. Achieving of this objective presents some considerable challenges in practice. Evaluating the performance of the single-phase GCI controller systems that is supplied with PV array DC under varying environmental conditions with the use of real PV panels in series or parallel according to the needs is practically impossible due to the lack of control over the irradiance and temperature and the requirement of large area, hence the use of PVEs has become compulsory [13]–[15]. A wide range of research papers have discussed the various controllers thoroughly by using conventional or advanced design techniques for the single-phase GCI systems [16]–[22].

The number of algorithms developed to extract the disturbing current and inject solely the smooth current to the grid has been proposed in literature. Among these the synchronous reference frame (SRF) and the instantaneous reactive power (IRP) theories are the most addressed applications in literature [23], [24]. The problem associated with the applications of these theories for the single phase PV system is the existing of the one phase variable only that obliges the creating of another virtual orthogonal variable with a 90 degree phase shift operation at the fundamental frequency [25]. In addition to those common theories, another proposed technique for the current control and the compensation of the selected harmonics is the adaptive control which contains several algorithms within itself such as the Least Mean Square (LMS) [26], the Decorrelation Normalized Least Mean Square (DNLMS) [27] and the Fractional Normalized Least Mean Square (FNLMS) [25]. Even though the adaptive control method has higher efficiency, its concept remains a challenge in terms of complexity and requirement of large number of calculations.

Alternatively, the Hysteresis Controller that is simple to implement and has fast response time with a drawback of generating variable switching frequency [28], [29], the Predictive Controller that tracks a reference signal with zero steady-state error with the drawbacks of its dependency on the accuracy of the system model to generate the reference current prediction precisely [30], [31], the Proportional-Integral (PI) Controller that is very simple and has the ease of implementation with drawbacks of inadequacy in tracking a sinusoidal reference signal with a zero steady-state error and having a poor disturbance rejection capability [29]. The Proportional-Resonant (PR) Controller proposes a solution to current control and harmonic mitigation problems associated with the aforementioned control techniques for the single-phase GCI systems [17], [19].

In this paper a novel PR controller is designed by using notch filter dynamics based symmetrical pole placement method. The proposed PR controller design technique offers an alternative with its unprecedented approach. It delivers an outstanding performance in current control and harmonic mitigation for the single-phase PV inverter systems. It consists of a resonant path and an external proportional gain. The external proportional gain stands for a regulator for varying system parameters such as inverter input voltage (V_{dc}) and filtering inductor (L_{inv}) shown in Figure 1 and can be altered easily for different applications. The resonant path has unity proportional gain and adjustable integral gain. These parameters are independent of V_{dc} and L_{inv} that means the proposed PR controller establishes more robustness and reduction in the computational complexity and consequently the proposed PR controller provides cost-effectiveness and simple implementation.

The paper is organized as follows. Section 2 introduces the overall system together with discussion and comparative analysis of designing and operational principle of the proposed PR controller. Section 3 is devoted to design and control of the DC-DC buck converter based PVE and MPPT algorithm (Perturb & Observe method). Section 4 contains simulation results and discussions.

II. PROPOSED PR-P CONTROLLER AND HARMONIC COMPANSATOR DESIGN

The PR controller has gained its popularity and become widely used current regulator for grid-connected single-phase systems [22], [32], [33]. The PR controller offers several advantages, such as resolving the computational burden and complexity due to removal of Park transformations, providing great convenience and simplicity to implement [34].

Figure 2 shows a circuit diagram of a single-phase PVE supported grid connected inverter. A buck DC-DC converter-based PV emulator is employed as the PV source. The PV source is connected to the grid using a full bridge DC-AC converter. The MPPT algorithm is employed to

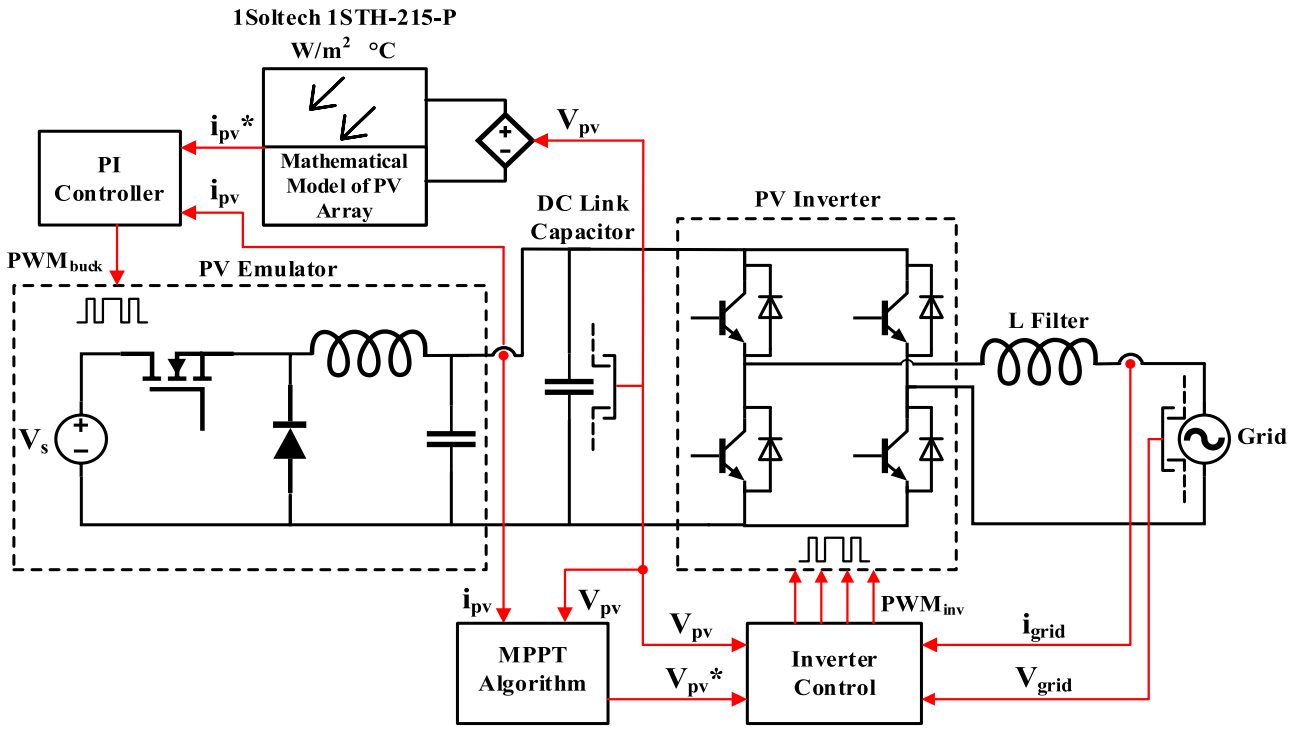

FIGURE 2. PVE based single phase grid-connected inverter system.

maintain the voltage at the maximum power point of the PV source, which is then input to the PV inverter so that the PV inverter can control the DC link voltage following the maximum power point voltage. The inverter also controls the inverter output current injection to the grid.

The ideal PR controller transfer function with its parameters proportional gain (K_P), integral gain (K_I) and the resonant frequency (ω_r) is represented by:

$$G_{PR}(s) = K_P + K_I \frac{s}{s^2 + \omega_r^2} \tag{5}$$

The ideal PR controller transfer function frequency response attains a phase shift and an infinite gain only at the resonant frequency (ω_r) that sets the steady-state error to zero and consequently enables to track sinusoidal reference signal efficiently at any specified resonant frequency. However, the ideal PR controller causes stability issues due to the infinite gain in applications [25]. Prevention of this problem is achieved with implementation of a non-ideal PR controller generated by introducing damping to the ideal transfer function [18], [19]. The non-ideal PR controller transfer function with addition of the bandwidth (ω_c) around the ac resonant frequency (ω_r) is represented by:

$$G_{PR}(s) = K_P + K_I \frac{2\omega_c s}{s^2 + 2\omega_c s + \omega_r^2} \tag{6}$$

The non-ideal PR controller produces a finite gain at the resonant frequency ω_r but it is still large enough to provide a very small steady-state error that is almost zero [19]. The single-phase inverter control process is comprised of three parts basically which are DC-link voltage controller, grid synchronization and current controller. Block diagram of the inverter control including all parts is given in Figure 4.

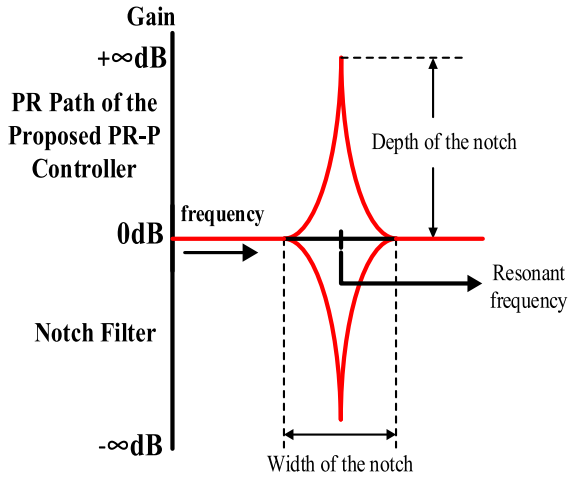

FIGURE 3. Notch filter and PR controller magnitude response in general form.

The general frequency magnitude response in dB of a notch filter and a PR controller is given in Figure 3. Resonant path of the proportional resonant (PR) controller is a notch filter. The logic behind the design process of the PR controller in the study is based on the ground of the notch filter dynamics and subsequently taking the reciprocal of the generated notch filter transfer functions at intended frequencies.

Proposed notch filter design process containing applied parameters and their functions is given in Figure 5.

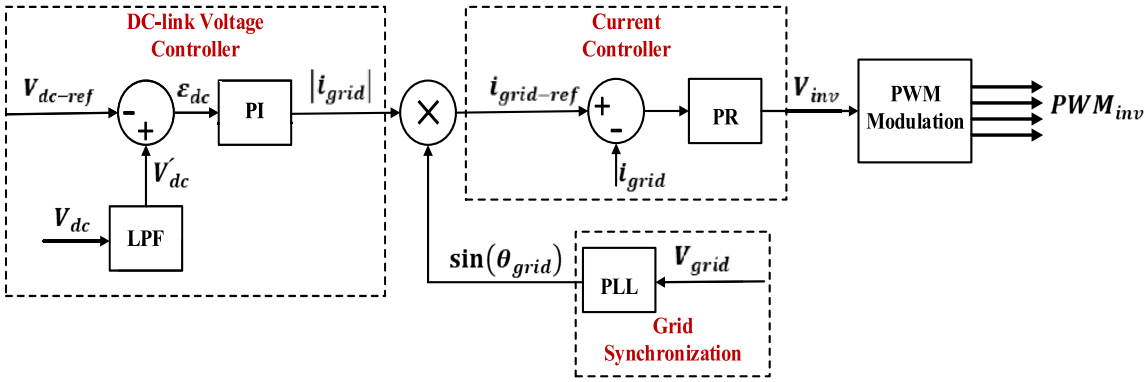

FIGURE 4. Block diagram of the inverter control.

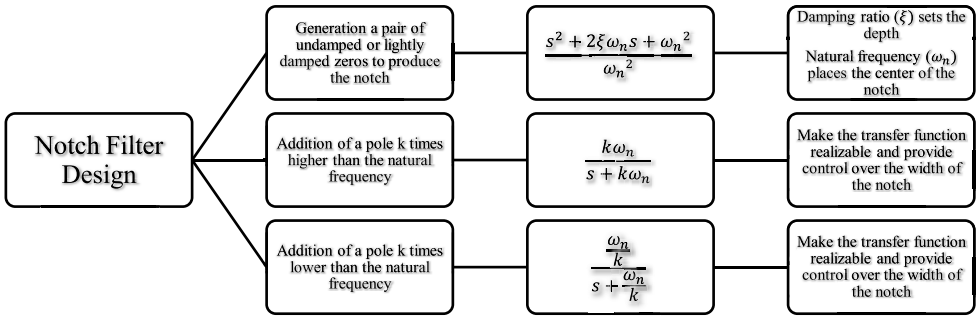

FIGURE 5. Notch filter design process.

Frequency response of the notch according to varying ξ and k is given in Figure 6. The parameter k is set to adjust the width of the notch, the damping ratio (ξ) is set to adjust the depth of the notch and the natural frequency (ω_n) is set to adjust the location of the notch that refers to resonant frequency for the PR controller. In [35], the value of ξ is recommended as 0.001 and the value of k is chosen in the range of 1 to 5 considering the location of dominant poles for providing sufficient damping and preventing high frequency issues [16].

First, the variable (k) will be defined as the ratio of each pole is away from the natural frequency. The larger value of k corresponds with a wider notch and can be adjusted according to the requirement. An unrealizable transfer function $G(s)$ that is lightly damped ($\xi = 0.0001$) pair of zeros centered at the natural frequency ($\omega_n = 50Hz$) that corresponds to the resonant frequency of the PR and the k (k = 2) for the application is given by:

$$G(s) = \frac{s^2 + 2\xi\omega_n s + \omega_n^2}{\omega_n^2} \tag{7}$$

First pole s_1 with a cut-off frequency k times larger than the natural frequency is given by:

$$s_1 = \frac{k\omega_n}{s + k\omega_n} \tag{8}$$

Second pole s_2 with a cut-off frequency k times smaller than the natural frequency is given by:

$$s_2 = \frac{\frac{\omega_n}{k}}{s + \frac{\omega_n}{k}} \tag{9}$$

Addition of both poles s_1 and s_2 to the transfer function $G(s)$ results in a formation of a second-order band-stop filter whose transfer function $G_{notch}(s)$ is given by:

$$\begin{aligned} G_{notch}(s) &= G(s).s_1.s_2 \\ &= \frac{s^2 + 2\xi\omega_n s + \omega_n^2}{\omega_n^2} \cdot \frac{k\omega_n}{s + k\omega_n} \cdot \frac{\frac{\omega_n}{k}}{s + \frac{\omega_n}{k}} \end{aligned} \tag{10}$$

Figure 7(a) shows the frequency response of the unrealizable transfer function that is constituted with a greater order of numerator than denominator given in (7). There is a gain rising at 40 dB/decade since there are two unanswered zeros, thus the high frequency signals are to pass through altered. Figure 7(b) shows that addition of a pole with a cut-off frequency that is k times larger than the natural frequency dragged the high frequency magnitude down by 20 dB/decade. Figure 7(c) shows that addition of a complementary pole with a cut-off frequency that is k times smaller than the natural frequency bended down the high frequency magnitude by 20 dB/decade to the zero dB.

The transfer function of the proposed PR controller $G_{PR}(s)$ is the reciprocal of the notch filter transfer function $G_{notch}(s)$

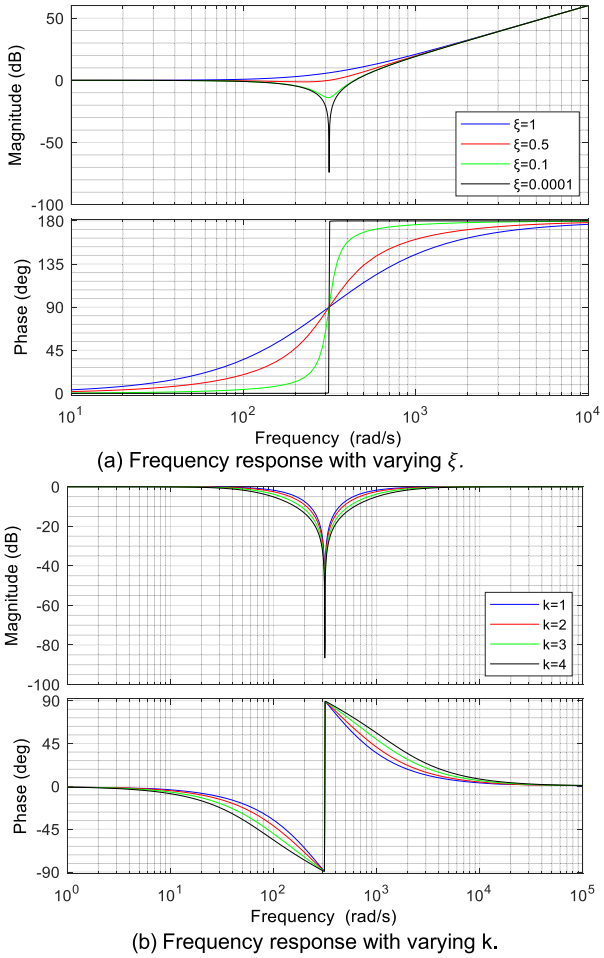

FIGURE 6. Phase and magnitude response of the notch filter.

is given in (11) and (12):

$$G_{PR}(s) = \frac{1}{G(s).s_1.s_2} = \frac{\omega_n^2}{s^2 + 2\xi\omega_n s + \omega_n^2} \cdot \frac{s + k\omega_n}{k\omega_n} \cdot \frac{s + \frac{\omega_n}{k}}{\frac{\omega_n}{k}} \quad (11)$$

$$G_{PR}(s) = \frac{9.87e04s^2 + 7.752e07s + 9.741e09}{9.87e04s^2 + 6201s + 9.741e09} \quad (12)$$

The magnitude and phase responses of the designed PR controller is given in Figure 8. The highest gain of the designed PR controller is 81.7 dB, and it occurs at the resonant frequency (ω_n= 50Hz). The phase response shows that the phase shift is zero for low and high frequencies.

Figure 8 indicates that for any arbitrary frequency ω_0, the gain of the PR controller transfer function $G_{PR}(j\omega_0)$ is at sufficient level without a phase shift for other frequencies, hence it can track sinusoidal reference signal without error.

A. THE PR CONTROLLER WITH HARMONIC COMPENSATOR

Grid connected inverter systems (GCI) mainly operate as transferring energy from the primary DC source such as PV arrays to the grid and hence inject harmonic currents

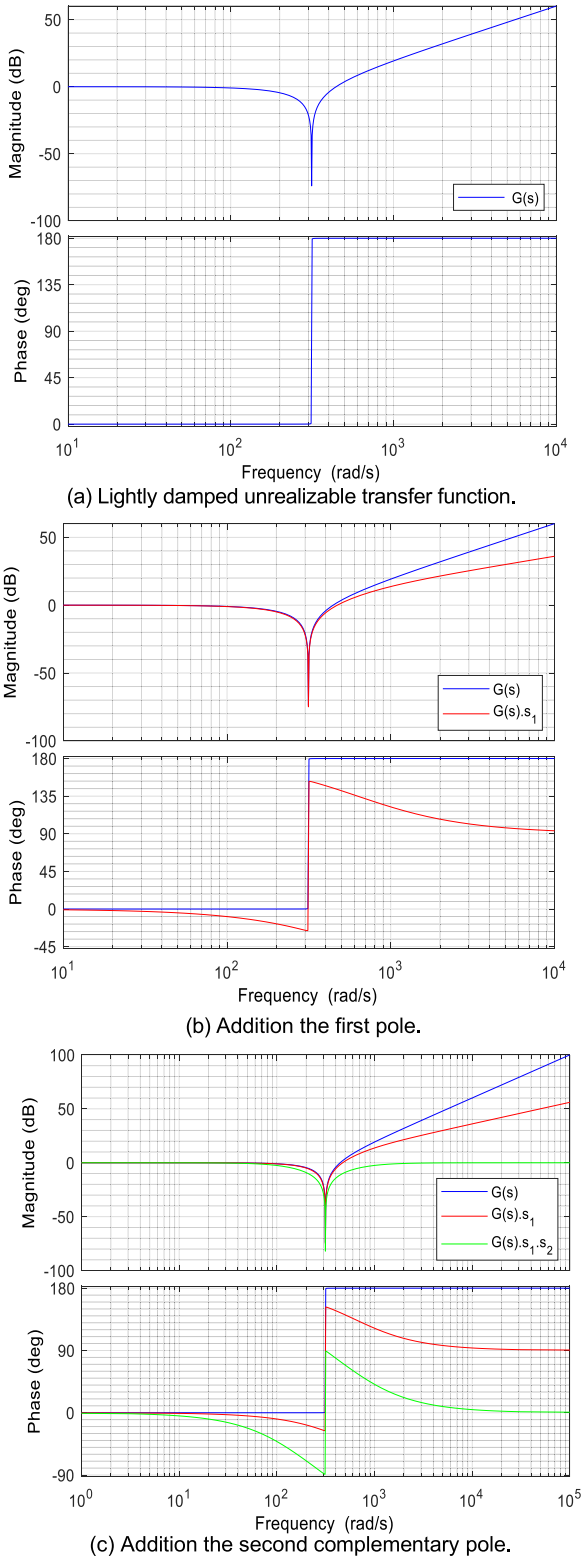

FIGURE 7. The notch filter dynamics-based PR controller.

to act as an active filter. In this regard, the reference signal is constituted of the sum of the fundamental component and some harmonic components (e.g., 3rd, 5th, 7th order harmonics). The PR controller assures zero steady-state error

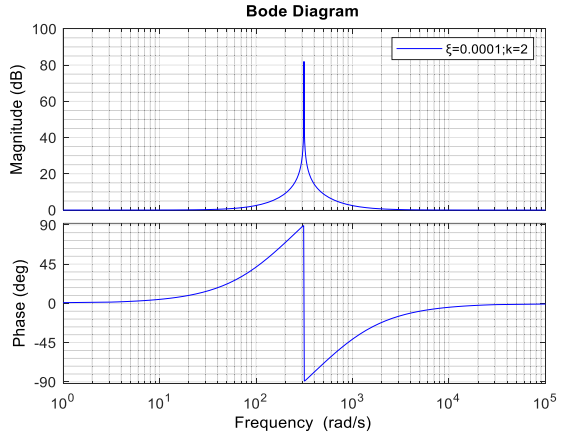

FIGURE 8. Magnitude and phase response of the proposed PR controller.

for any harmonic components at issue by implementing additional resonant paths to the controller. The block diagram of the general system with a PR controller that consists of n-resonant paths is given in Figure 9:

General form of the selective harmonics' compensator transfer function $G_H(s)$ is represented by:

$$G_H(s) = \sum_{h=3,5,7,\ldots} \frac{(h\omega_n)^2}{s^2 + 2\xi h\omega_n s + (h\omega_n)^2} \times \frac{s + kh\omega_n}{kh\omega_n} \times \frac{s + \frac{h\omega_n}{k}}{\frac{h\omega_n}{k}} \quad (13)$$

In the design of objective resonant paths, the same pole placement notch filter dynamics-based technique that is previously stated will be implemented. The only changing parameters is the resonant frequencies. The resonant frequency for the fundamental component is 50 Hz (ω_n), for the 3rd order harmonic component 150 Hz ($3\omega_n$) and for the 5th order harmonic component 250 Hz ($5\omega_n$). The magnitude and phase responses of the designed PR controller with 3rd and 5th harmonics compensator is given in Figure 10:

B. COMPARATIVE ANALYSIS OF THE PROPOSED PR-P CONTROLLER

In [36], the PR controller main frame that is the resonant path ($H_R(s)$), fundamental parameters proportional gain (K_P) and (K_I) for the single-phase grid connected full-bridge inverter are formulized as:

$$H_R(s) = \frac{k_r B_r s}{s^2 + 2B_r s + \omega_r^2} \quad (14)$$

$$K_P = \frac{(2\xi + 1)\sqrt{(2\xi + 1)}\omega_r L_{inv}}{V_{dc}} \quad (15)$$

$$K_I = \frac{\omega_r^2 L_{inv}\left[(2\xi + 1)^2 - 1\right]}{2V_{dc}} \quad (16)$$

Equation (14),(15),(16) consist of various parameters that are resonant gain (k_r), resonant angular bandwidth (B_r), resonant angular frequency (ω_r), damping ratio (ξ), inverter output filter inductance (L_{inv}), inverter input voltage (V_{dc}) and constitute commonly used non-ideal PR controller transfer function design given in (6). In [37], it is presented that the most frequently used conventional PR controller poses problems in the presence of non-linear load and weak grid condition. In [19] and [38], studies were performed by utilizing this formula and it provides consistent results in terms of transient response and selective harmonics mitigation but the number of parameters used in the design process increases the complexity of the controller. Moreover, dependency on the variables such as (L_{inv}) and (V_{dc}) in the calculations of the K_P and K_I decreases the robustness of the controller as these variables are likely to change over time or to vary during operations. On the contrary, the PR path of the proposed PR-P controller design process is independent of these variables. Rearranging the PR path of the controller transfer function in (11) gives:

$$G_{PR}(s) = 1 + \frac{\left(\frac{\omega_n}{k} + k\omega_n - 2\xi\omega_n\right)s}{s^2 + 2\xi\omega_n s + \omega_n^2} \quad (17)$$

The proposed controller resonant path has a constant unity proportional gain K_P and addition of each harmonic reduction component increases it 1. K_I depends only on three parameters that are k, ω_n and ξ. The assessment of the PR path of the proposed controller indicated that using $G_{PR}(s)$ obtained in (17) meets the IEEE Std 519-1992 standards with a sufficiently good transient response. Addition of scheduled proportional gain ($K_{P(ex)}$) determined by loop shaping method to the resonant path PR considering system uncertainties, weak grid condition, non-linear loads and grid fault has resolved the problems associated with the use of conventional PR controller. In this regard, the proposed PR-P controller can be considered as a system consisting of unity proportional gain resonant path $G_{PR}(s)$ and controllable variable $K_{P(ex)}$ given in Figure 11(a). The overall current control and selective harmonic mitigation scheme for GCI systems is given in Figure 11(b).

C. TUNING THE SCHEDULED GAIN OF THE PROPOSED CONTROLLER

Large signal average model of the full-bridge inverter given as:

$$L\frac{d\langle\hat{i}_{inv}\rangle}{dt} = (2d - 1)V_{dc} - v_{ac} \quad (18)$$

where L, $\langle\hat{\boldsymbol{i}}_{\boldsymbol{inv}}\rangle$, d, $\boldsymbol{V_{dc}}$ and $\boldsymbol{v_{ac}}$ are the inductance of the inverter filter, duty cycle of the inverter PWM signal, input voltage of the inverter and grid voltage, respectively. Assuming that there is no small signal variation in $\boldsymbol{v_{ac}}$ as the control input is the duty cycle, linearization of (18) gives:

$$L\frac{d\hat{i}_{inv}}{dt} = 2V_{dc}\hat{d} \quad (19)$$

Laplace transform of (19) gives small-signal transfer function of the inverter as:

$$sL\hat{i}_{inv} = 2V_{dc}\hat{d}$$

$$G_{inv}(s) = \frac{\hat{i}_{inv}}{\hat{d}} = \frac{2V_{dc}}{Ls} \quad (20)$$

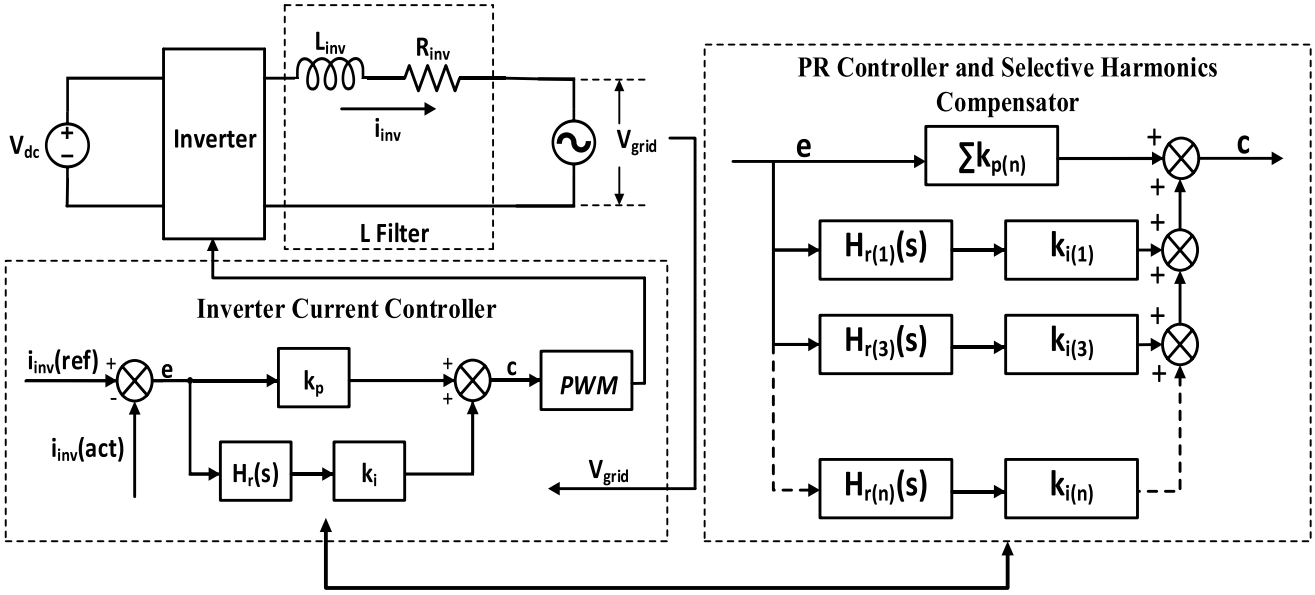

FIGURE 9. The PR controller with n-resonant paths.

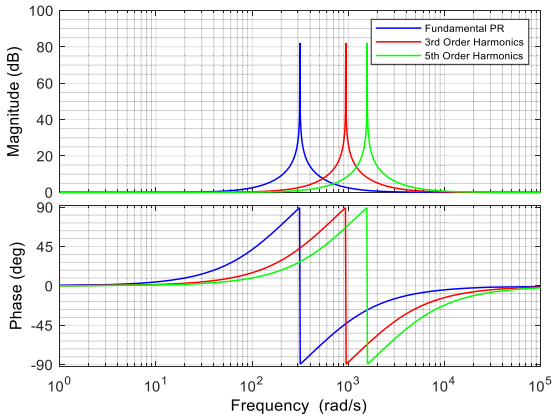

FIGURE 10. Magnitude and phase response of the designed PR controller with 3rd and 5th harmonic components compensator.

The power inverter input voltage is 400 V and it is connected to the grid via L filter whose inductance is 1 mH. Accordingly, substituting these values in (20) yields:

$$G_{inv}(s) = \frac{\hat{i}_{inv}}{\hat{d}} = \frac{800}{0.001s} \tag{21}$$

Magnitude and phase response of the loop transfer function that is $\boldsymbol{G_{PRP}}(s)$ times $\boldsymbol{G_{inv}}(s)$ with varying $\boldsymbol{K_{P(ex)}}$ is given in Figure 12.

The look-up table breakout points correspond to closed-loop current feedback error and the outputs are retrieved from a given set of breakout points (input values) as scheduling variables for the constant $\boldsymbol{K_{P(ex)}}$ whose value is determined as 100 according to the loop transfer function magnitude and phase response given in Figure 13.

The look-up table method is based on linear interpolation between two consecutive elements of the table if the error signal does not match a breakout point and extrapolation if the error is not falling within the range of breakout values. Average current mode control loop of the inverter assuming

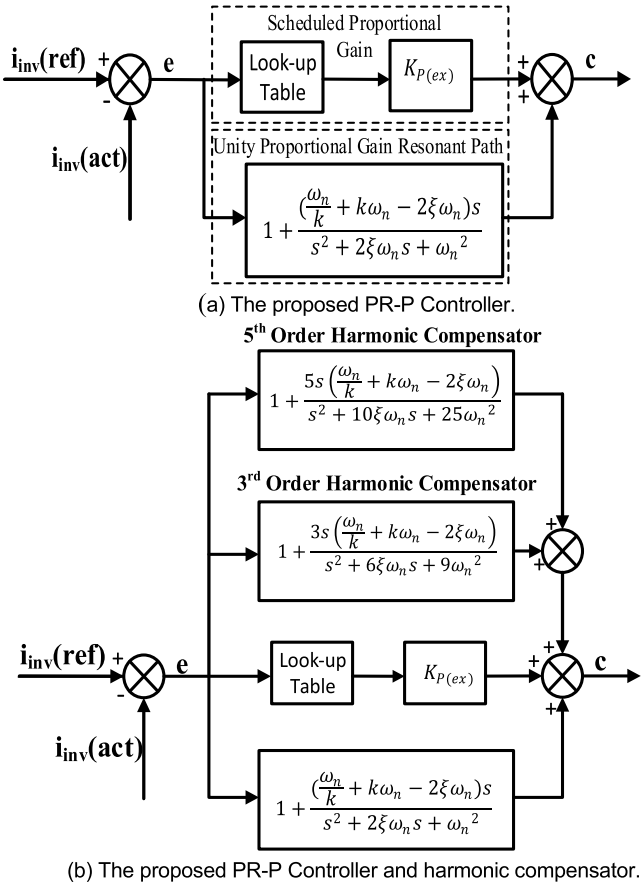

(a) The proposed PR-P Controller.

(b) The proposed PR-P Controller and harmonic compensator.

FIGURE 11. The proposed PR-P controller and harmonic compensator.

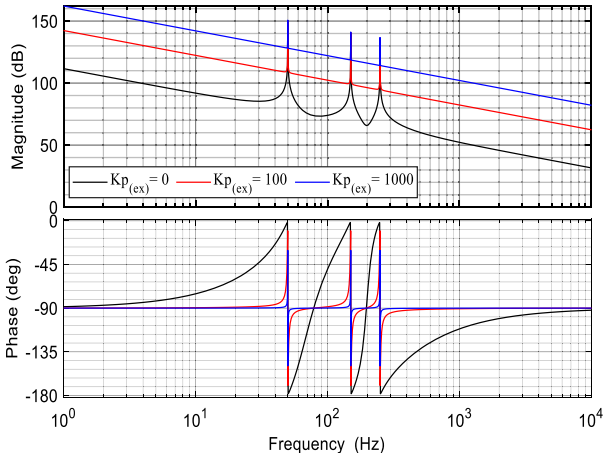

FIGURE 12. Magnitude and phase response of the loop transfer function with varying $K_{P(ex)}$.

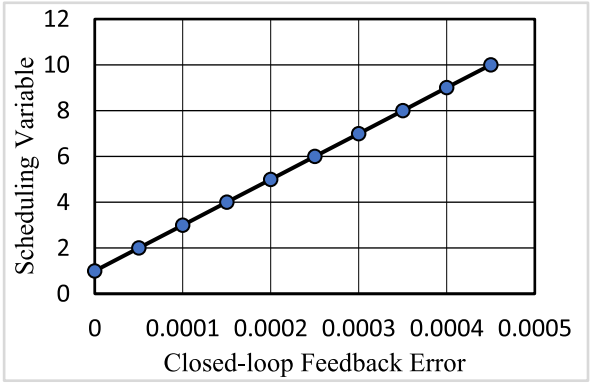

FIGURE 13. Dynamic of the look-up table.

that pulse width modulator (PWM) gain 4 V, sensing resistor R_F 1 Ω with all harmonics injecting is given in Figure 14.

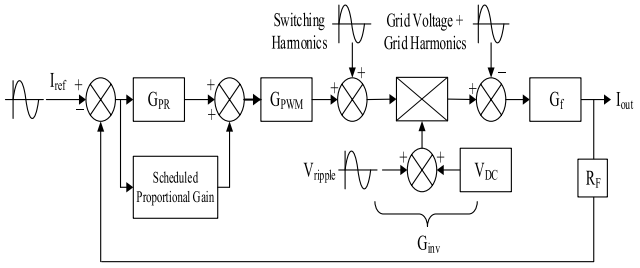

FIGURE 14. Inverter average current mode compensator design loop.

Inverter average current control feedback system outputs for implementation of different controllers are given in Figure 15. While most frequently used PI and conventional PR control techniques perform poorly in the presence of harmonics, the proposed PR-P controller follows its reference with negligible steady-state error.

III. PVE AND MPPT ALGORITHM

The current-voltage (I-V) and the power-voltage (P-V) characteristics curves of the PV cells are heavily dependent on changing environmental conditions such as irradiance and

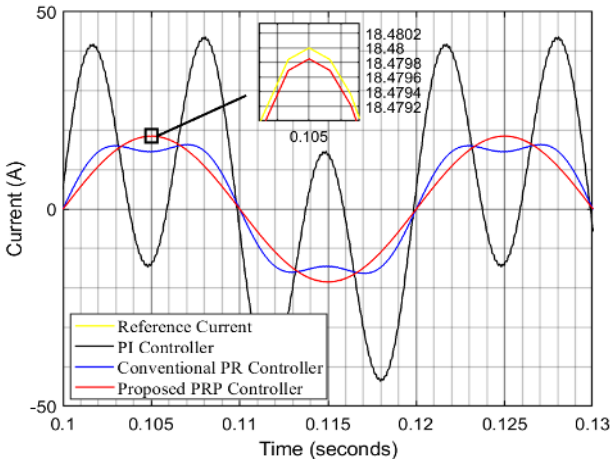

FIGURE 15. Reference tracking performance of the various controller in the presence of harmonics.

temperature [39]. In accordance with the efficiency-based aforesaid objectives in the introduction, maintaining the characteristic curves at a specific point that is known as the maximum power point (MPP) is required [40]. In this regard, maximum power point tracking (MPPT) concepts are employed at PV array in practice to harvest the maximum power from the PV module or array under various irradiance and temperature conditions [41]. Tracking performance of the MPPT algorithms has great importance, hence it has been the main subject of many studies and different methods are developed in consequence [42]–[44]. Development and improvement of MPPT techniques with the real PV panels posed some challenges such as being inability to control the environmental factors, requirement of wide space and cost [13], [45]. At this point, photovoltaic emulators (PVE) have become the essential part of the PV applications in terms of development of the MPPT algorithms [46]. The working principle of the PVE is based on generating the explicit dynamics of the I-V and P-V characteristics curves of the real PV panel at issue [14], [47]. It is worth noting that whilst the objective PVE delivers a good performance by itself, it may exhibit undesirable behaviors as a result of interfacing with some switch mode power supplies that constitute the indispensable of the PV power generation and delivering systems or it may not reflect the same PV characteristics through the variance of the irradiance and the temperature [48], [49]. Referring to the previous works taking part in literature, many different PVE modelling and simulations have been conducted and these PVEs have designed with pure resistive load and their I-V and P-V curves compared with the real PV panel or they are integrated with a Boost Converter for the MPPT applications, [13], [15], [48], [50].

A. DESIGN PROCEDURE OF THE PVE

The paper proposed scrutinization of buck converter based PVE single phase grid-connected H-bridge inverter system with a maximum power point tracking (MPPT),

TABLE 1. The emulated PV module (1Soltech 1STH-215-P) parameters.

Parameter	Value
Maximum Power (W)	231.15
Open Circuit Voltage V_{OC} (V)	36.3
Voltage at Maximum Power Point V_{MPP} (V)	29
Temperature Coefficient of V_{OC} (%/deg.C)	-0.36099
Cells per Module (Ncell)	60
Short-circuit Current I_{SC} (A)	7.84
Current at Maximum Power Point I_{MPP} (A)	7.35
Temperature Coefficient of I_{SC} (%/deg.C)	0.102

a proportional-resonant-proportional controller (PR-P) for the purpose of the current control as well as 3rd and 5th order harmonics mitigation with the aid of multiple domains of MATLAB and Simulink. The emulated PV module is 1Soltech 1STH-215-P with parameter given in Table 1.

The proposed buck converter based PVE and its control structure block diagram is given in Figure 16.

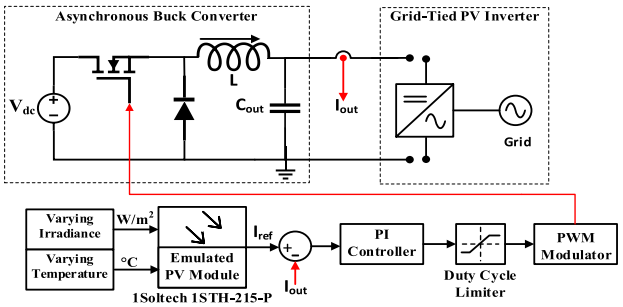

FIGURE 16. The Proposed buck converter based PVE and control structure.

It takes an input voltage (Vdc) of 48 volts and converts it into an output voltage of 36.3 volts. The switching frequency is 10 kHz. The minimum load resistance R_{min} is 4.6301 ohm (corresponds to the maximum load condition). In the continuous conduction mode (CCM) operation of the PVE, the maximum ripple allowed in the inductor is 20% of the average inductor current and the maximum load. The maximum ripple in the capacitor is plus and minus 2% of the average output voltage.

The output voltage (V_{out}) of the PVE corresponding to the inverter input voltage is determined as 400 V in this application, thus the PVE is considered as the series connection of 14 PV modules that results in approximately 3 kW power generation.

B. CALCULATIONS THE VALUES OF PV EMULATOR COMPONENTS

The steady state duty cycle of the plant is represented by:

$$D = \frac{V_{out}}{V_{in}} \tag{22}$$

TABLE 2. Calculated values of the PVE parameters and components.

Parameters and Components	Value
Steady-state Duty Cycle (D)	0.7563
Maximum Average Inductor Current (A)	7.84
Maximum Average Inductor Current Ripple (A)	1.568
Inductor Value (mH)	0.5642
Output Voltage Ripple (V)	1.452
Capacitor Value (μF)	13.4989

The maximum average inductor current is represented by:

$$I_{L,avg,max} = \frac{V_{out}}{R_{min}} \tag{23}$$

The maximum average inductor ripple current is the 20% of the average current that is represented by:

$$\Delta I_L = 0.2 \times I_{L,avg,max} \tag{24}$$

Inductance value L of the inductor is represented by:

$$L = \frac{V_{in}\,(1-D)\,D}{f_{sw}\Delta I_L} \tag{25}$$

Capacitor ΔV_C or output voltage ripple ΔV_{out} is the ±2% of the average output voltage is represented by:

$$\Delta V_C = \Delta V_{out} = 0.04 \times V_{out} \tag{26}$$

Capacitance value C of the capacitor is represented by:

$$C = \frac{V_{in}\,(1-D)\,D}{8Lf_{sw}^2\Delta V_C} \tag{27}$$

The calculated values of the PV emulator parameters and components are given in Table 2:

C. PROPORTIONAL-INTEGRAL CONTROLLER DESIGN FOR THE PVE

Analysis of the plant for predicting its response and observing its behaviors in both the time and frequency domains requires obtaining its mathematical model properly. In this regard, control systems are designed and implemented to improve important dynamic properties of the plant such as stability, response time, steady-state error, oscillations that constitute the transient and the steady-state responses of the system.

Transfer function of the intended buck converter based PVE in terms of duty ratio (d(s)) to inductor current (i_L(s)) given in (28) and (29) is derived by using dynamic (AC small signal) state-space averaging technique.

$$G_{PVE}(s) = \frac{i_L(s)}{d(s)} = \frac{V_{in}}{L}.\frac{s + \frac{1}{R_{Load}C}}{s^2 + \frac{s}{R_{Load}C} + \frac{1}{LC}} \tag{28}$$

$$G_{PVE}(s) = 8.5063e4.\frac{s + 1.6e4}{s^2 + 1600s + 1.3128e8} \tag{29}$$

The Proportional-Integral (PI) feedback compensator structure is a controller that is widely used due to the properties of being simple to implement, easily comprehensible,

very understandable and its effectiveness. The unity feedback structure of the proposed PVE system is given in Figure 17:

The closed-loop transfer function of inductor current to the duty ratio for the unity-feedback system with a proportional-integral control is the following:

$$G_{CL}(s) = \frac{V_{in}K_p}{L}[s^2 + s\left(\frac{1}{CR_{Load}} + \frac{K_i}{K_p}\right) + \frac{K_i}{K_pCR_{Load}}] \div [s^3 + s^2\left(\frac{1}{CR_{Load}} + \frac{K_pV_{in}}{L}\right) + s\left(\frac{1}{CL} + \frac{K_pV_{in}}{CLR_{Load}} + \frac{K_iV_{in}}{L}\right) + K_iV_{in}] \quad (30)$$

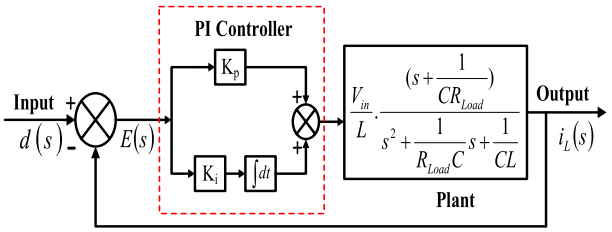

FIGURE 17. The unity feedback control structure of the PVE.

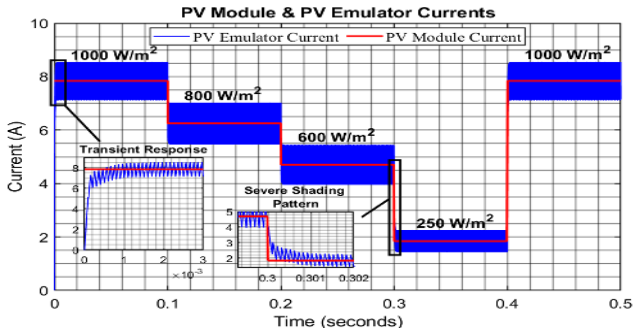

FIGURE 18. The emulated PV module and PVE currents.

Considering the stability criteria of a switch mode power supply (SMPS) which are the crossover (cutoff or break) frequency between the range of 1/10th to 1/8th of the switching frequency, the phase margin larger than 45 degree, the gain margin larger than 10 dB and the slope of the gain curve at the crossover frequency is about −20 dB/decade, K_p and K_i values are calculated as 0.21 and 709, respectively. Emulated PV module (1Soltech 1STH-215-P) and the proposed PV emulator controlled by the designed PI controller current waveforms for varying irradiance of 1000 W/m^2, 800 W/m^2, 600 W/m^2 and 250 W/m^2 (severe shading pattern) that correspond to 7.84 A, 6.272 A, 4.704 A and 1.844 A, respectively are given in Figure 18.

D. PERTURB AND OBSERVE (P&O) MPPT ALGORITHM

The P&O MPPT technique is one of the most basic and commonly used algorithms in PV systems. Implementation of the algorithm depends on the trial-and-error method in pursuit of maximum power point (MPP) and tracking it [39]. The method is required to measure only the PV array's current and voltage to calculate the power and perturbing the duty cycle based on the comparison of the initial and present values of the power and voltage until reaching the MPP occurring at MPP voltage (VMPP) [51]. The use of current and voltage sensors only causes relatively big reduction in the operational cost. Moreover, its convenience and compatibility with the grid-tied converter systems due to effective regulation of the output voltage and dynamic performance in terms of fast response time is considered as the notable feature of the algorithm [44], [48]. The flowchart of the algorithm and accordingly its execution on the power-voltage (P-V) characteristics curve of the PV module is given in Figure 19.

The parameters of the developed algorithm are 400 V initial value of the voltage reference that corresponds VMPP and the input voltage of the inverter, 410 V upper limit and 390 V lower limit. Increment value used to increase or to decrease the voltage is 0.003 V.

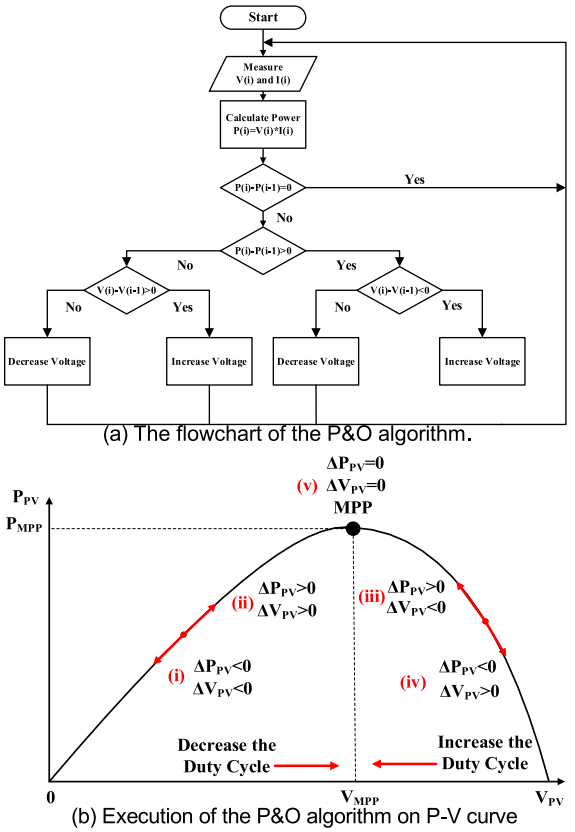

FIGURE 19. Perturb and observe (P&O) algorithm.

IV. SIMULATION RESULTS AND DISCUSSION

This paper proposed a novel approach to design a PR-P controller that is based on changing notch filter dynamics by implementing of two symmetrical poles to both sides of the resonant frequency at which the control is aimed and taking the reciprocal of the derived transfer function. In addition to this, the performance of the PR-P controller is validated under real-like developed switch mode power supply (SMPS) PVE sourced single-phase GCI system.

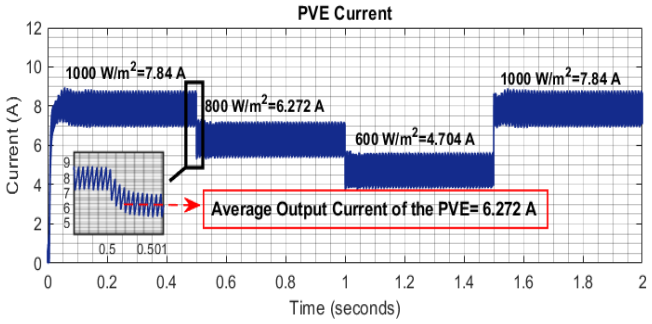

FIGURE 20. The PVE current for varying irradiance.

The simulation of the PVE supported single phase grid connected inverter with the proposed PR-P controller was performed in MATLAB/Simulink by assuming inverter switching frequency is 6 kHz, peak value of the grid voltage is 340 V, and the frequency is 50 Hz. Figure 20 shows the current output of the PVE under varying irradiance. The PI controller for the PVE reveals good performance in terms of transient response and tracking the emulated PV module current given in Table 1. The system reaches steady state in less than 1 millisecond in line with the reference current.

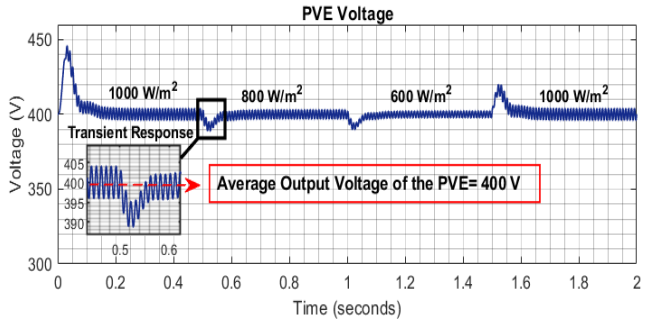

FIGURE 21. The PVE voltage for varying irradiance.

Figure 21 shows the voltage output of the PVE under varying irradiance. The designed P&O MPPT algorithm performs well and tracks the reference voltage of 400 V effectually if there is not big variation in the irradiance. The reason for the poor transient response for the abrupt and significant shift in the irradiance occurred at the very beginning when the irradiance changed from 0 to 1000 W/m^2 and from 600 W/m^2 to 1000 W/m^2 at 1.2nd second is due to the fixed step size of $\Delta V = 0.003$ V.

Figure 22(a) presents the inverter output current and reference current behaviors in both stages of stepping from a null current to a sinusoidal waveform and transient response after the sinusoidal waveform. The proposed PR-P controller functions properly and makes the inverter current follows the reference current with negligible steady-state error and consequently maintains the grid voltage and current in phase as shown in Figure 22(b). The transient period takes approximately 0.06 second with insignificant oscillation in the inverter current that denotes the rapid response of the controller.

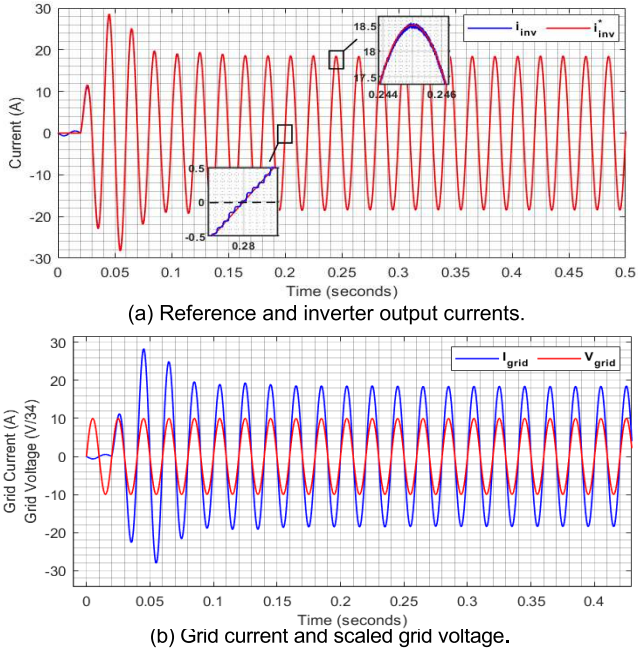

(a) Reference and inverter output currents.

(b) Grid current and scaled grid voltage.

FIGURE 22. System outputs with the use of proposed PR-P controller.

TABLE 3. Implementing of the unscheduled PR-P controller with harmonic compensator.

Magnitude of Harmonic Distortion (% of Fundamental)	PR-P controller without scheduled proportional gain $K_{p(ex)}$		
	Without harmonic compensator	Implementing 3rd order harmonic compensator	Implementing 3rd and 5th order harmonic compensators
THD	4.68	4.65	4.64
3rd order harmonic component	0.4149	0.0008684	0.001779
5th order harmonic component	0.1519	0.06788	0.0005461
7th order harmonic component	0.02581	0.03124	0.04333
9th order harmonic component	0.137	0.07815	0.04409
11th order harmonic compoennt	0.02715	0.08445	0.03253

Power generation for varying irradiance and its deliver through an inverter in terms of active and reactive powers are giving in Figure 23. The power generation, conditioning and its deliver to the grid process is accomplished efficiently with zero reactive power. The transient regime stems from the output voltage waveform of the PVE as indicated in Figure 21.

Table 3 presents total harmonic distortion (THD) of the grid current for varying frequencies for the cases

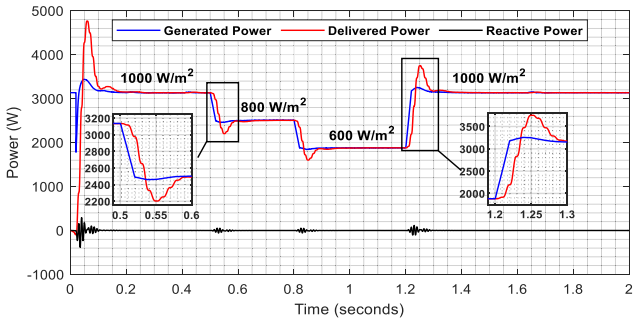

FIGURE 23. Generated power with delivered and reactive powers.

TABLE 4. Constant proportional gain ($K_{P(ex)} = 20$) PR-P controller with 3rd and 5th order harmonics compensator with varying Inverter output inductor values.

Magnitude of Harmonic Distortion (% of Fundamental)	PR-P controller with constant proportional gain $K_{p(ex)}$=20 with 3rd and 5th order harmonic compensators		
	L_{inv}= 1 mH	L_{inv}= 3 mH	L_{inv}= 5 mH
THD	1.90	1.79	1.64
3rd order harmonic component	0.001909	0.00176	0.002072
5th order harmonic component	0.001138	0.001344	0.001361
7th order harmonic component	0.2354	0.268	0.1677
9th order harmonic component	0.2003	0.1931	0.1202
11th order harmonic compoennt	0.1488	0.1232	0.07186

of implementing unscheduled PR-P controller itself, PR-P controller with 3rd order harmonic compensator and PR-P controller with both 3rd and 5th order harmonic compensator assuming that $K_{P(ex)}$ is zero.

In Table 4, the PR-P controller and 3rd and 5th order harmonics compensators are implemented with $K_{P(ex)}$ value of 20 by considering variation in the inverter output inductor values.

In Figure 22, the same application is carried out with a constant inductance and varying $K_{P(ex)}$ values. The results shows that the performance of the proposed control scheme is satisfactory and in compliance with the IEEE Std 519-1992.

The main drawbacks of the PI controller in single phase GCI systems are insufficiency in removing the steady-state error in stationary reference frame shown in Figure 25 and being incapable of selective harmonics mitigation. In Figure 24, closed loop errors of PR and PI controllers are presented. The 3rd order harmonic component is eliminated within a quarter second with the proposed PR controller. However, the use of PI controller results in a constant error regarding the 3rd order harmonic component in the grid current. The PR controller is more efficient in terms of harmonic compensation and removing the steady-state error.

Performance validation of the proposed PR-P controller involves checking its efficiency compared with PI controller

TABLE 5. Constant inverter output filtering inductance (L = 3 mH) with varying $K_{P(ex)}$ values PR-P controller with 3rd and 5th order harmonics compensators.

Magnitude of Harmonic Distortion (% of Fundamental)	PR-P controller with scheduled proportional gain $K_{p(ex)}$ + 3rd and 5th order harmonic compansators Constant Inverter Filtering Inductance L_{inv}= 3 mH		
	$K_{p(ex)}$= 0	$K_{p(ex)}$= 10	$K_{p(ex)}$= 20
THD	4.64	0.49	0.49
3rd order harmonic component	0.00389	0.04725	0.04776
5th order harmonic component	0.001712	0.03015	0.03001
7th order harmonic component	0.04379	0.02842	0.02831
9th order harmonic component	0.04727	0.008881	0.008885
11th order harmonic compoennt	0.03033	0.0004584	0.00172

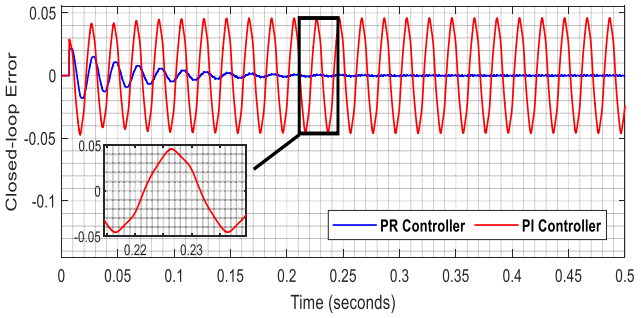

FIGURE 24. Closed-loop error in terms of 3rd order harmonics.

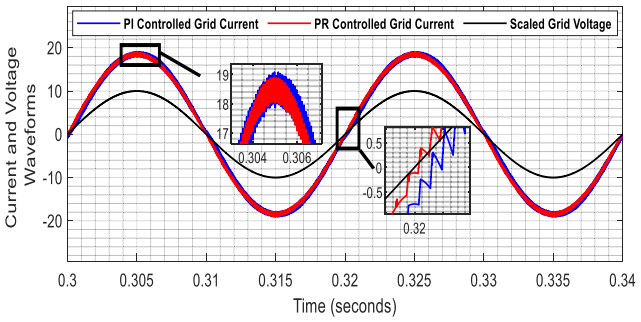

FIGURE 25. PR-P and PI controlled grid currents with scaled grid voltage.

in the presence of severe shading pattern, non-linear load and weak grid that constitute the main concerns in grid connected applications. The general structure of the overall system given in Figure 26.

Parameters of the buck converter based PVE sourced single phase grid connected inverter system is given in Table 6.

Single phase transmission line with lumped parameters is given in Table 7.

Figure 27 shows that PI current control of the PVE sourced single phase grid-tied inverter resulted in deterioration and

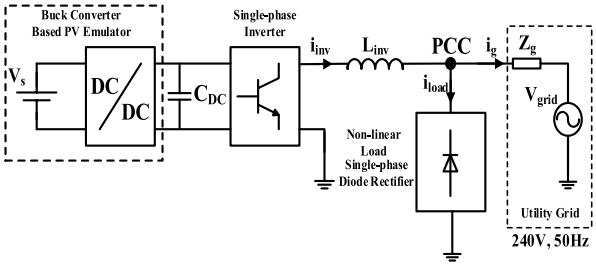

FIGURE 26. Single-phase PVE sourced grid-connected inverter system in the presence of non-linear load and weak grid.

TABLE 6. The simulated system parameters.

Parameter	Value
Grid phase voltage (rms)	V_{grid}=240V
Grid frequency	f=50Hz
Inverter filtering inductance	L_{inv}=3mH
Average DC-bus voltage	V_{dc}=400V
DC-bus capacitor	C_{DC}=3000μF
Inverter switching frequency	f_{sw}=6kHz

TABLE 7. Transmission line parameters.

Transmission Line Parameters	Value
Resistance per unit length	0.2568 Ohms/km
Inductance per unit length	2 mH/km
Capacitance per unit length	8.6 nF/km
Line lenght	10 km

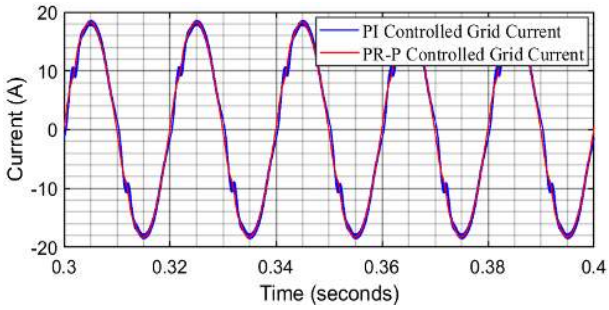

FIGURE 27. PI and PR-P controlled grid currents.

distortion of the current while proposed PR-P controller gives better results in the presence of non-linear load and weak grid.

Figure 28 indicates that closed-loop error in terms of 3rd order harmonic component is mitigated by the proposed PR-P controller effectively while PI controller is inefficient of selective harmonic compensation. Additionally, the proposed PR-P controller responds swiftly to sudden large irradiance change with less oscillation compared to PI controller.

Table 8 shows low order harmonic distortions of grid current and voltage waveforms for PI and proposed PR-P

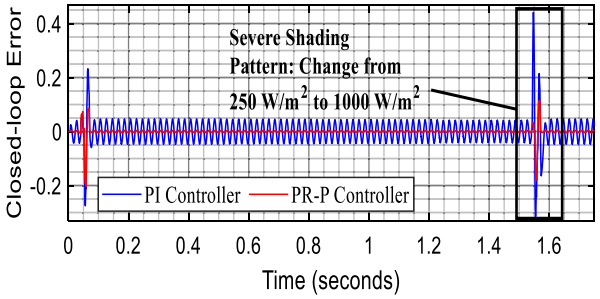

FIGURE 28. 3rd order harmonic component closed-loop error.

TABLE 8. Comparison of harmonic distortions for PI and PR-P controller in the presence of non-linear load and weak grid.

Magnitude of Harmonic Distortion (% of Fundamental)	Harmonic Distortion in the Presence of Non-linear Load and Weak Grid			
	PI Controller		PR-P Controller	
	Grid Voltage	Grid Current	Grid Voltage	Grid Current
THD	9.22	6.59	3.52	1.88
3rd order harmonic component	0.6419	1.054	0.2416	0.2843
5th order harmonic component	1.442	1.655	0.4919	0.5301
7th order harmonic component	3.023	3.227	0.7997	0.7814
9th order harmonic component	3.211	3.331	1.046	1.015
11th order harmonic compoennt	2.444	2.519	0.9266	0.9263

controller in the presence of non-linear load and weak grid. The THD value of grid current is 6.59 % with PI controller; however, the THD value of the grid current 1.88 % with the proposed PR-P controller. The THD value of the grid current is reduced 79.81% with the use of proposed PR-P controller. The results verify the effectiveness of the proposed PR-P control method in attenuation of the disturbing current in the presence of non-linear load and weak grid condition.

A. SENSITIVITY ANALYSIS AND ROBUSTNESS OF PROPOSED SYSTEM

Sensitivity analysis is indispensable part of modern control system theory and design applications. It is crucial to choose controller parameters in such a manner that the closed-loop system assures design requirements even though variations in process dynamics occur during operation. In this paper, a full-bridge inverter is fed by a buck converter-based PV emulator whose output voltage is kept constant at 400 V with P&O MPPT method that is the nominal average DC-bus voltage V_{dc} for the inverter and the inverter filtering inductance L_{inv} is determined as 1 mH. Variations in these parameters are bound to happen due to environmental and process-based factors. Closed-loop transfer function of the proposed PR-P controller inverter system in s-domain using unity negative feedback can be rewritten replacing the $2V_{dc}$ and L_{inv} in small-signal transfer function of the inverter

obtained in (20) with α and β respectively as:

$$T(s) = \frac{N(s)}{D(s)} = \frac{(G_{PR}(s) + K_{P(ex)})G_{inv}(s)}{1 + (G_{PR}(s) + K_{P(ex)})G_{inv}(s)} = \frac{(1 + \frac{(\frac{\omega_n}{k} + k\omega_n - 2\xi\omega_n)s}{s^2 + 2\xi\omega_n s + \omega_n^2} + K_{P(ex)})\frac{\alpha}{\beta s}}{1 + (1 + \frac{(\frac{\omega_n}{k} + k\omega_n - 2\xi\omega_n)s}{s^2 + 2\xi\omega_n s + \omega_n^2} + K_{P(ex)})\frac{\alpha}{\beta s}} \quad (31)$$

Sensitivity of the closed-loop transfer function due to α ($2V_{dc}$) that is the numerator of the inverter transfer function $G_{inv}(s)$ is derived as:

$$S_\alpha^T(s) = \frac{\alpha}{T(s)} \frac{\partial T(s)}{\partial \alpha}\Big|_{\alpha=800} \quad (32)$$

$$S_\alpha^T(s) = \frac{\alpha}{N(s)} \frac{\partial N(s)}{\partial \alpha} - \frac{\alpha}{D(s)} \frac{\partial D(s)}{\partial \alpha}\Big|_{\substack{\alpha=800 \\ \beta=0.001}} \quad (33)$$

Sensitivity of the closed-loop transfer function due to β (L_{inv}) that is the denominator of the inverter transfer function $G_{inv}(s)$ is derived as:

$$S_\beta^T(s) = \frac{\beta}{T(s)} \frac{\partial T(s)}{\partial \beta}\Big|_{\beta=0.001} \quad (34)$$

$$S_\beta^T(s) = \frac{\beta}{N(s)} \frac{\partial N(s)}{\partial \beta} - \frac{\beta}{D(s)} \frac{\partial D(s)}{\partial \beta}\Big|_{\substack{\beta=0.001 \\ \alpha=800}} \quad (35)$$

The system sensitivity to variations in α and β in terms of magnitude in dB obtained from (33) and (35) for varying irradiance is plotted in Figure 29. The system is more sensitive to the variations in inverter filtering inductance compared to inverter input voltage, but both meet the requirement that is having small nominal sensitivity peak for low frequencies for better reference tracking and disturbance rejection.

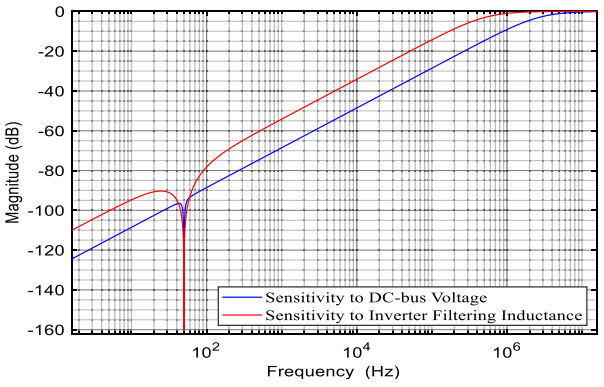

FIGURE 29. System sensitivity to DC-bus voltage and inverter filtering inductance.

A robust system must be capable of meeting requirements that are ensuring the stability of a system and performance measures even in the presence of uncertainties, disturbance, and noise. Sensitivity and complementary sensitivity analysis for overall system are one of the most important useful concepts for a robust control. Nominal sensitivity peak of a system is given as:

$$M_s = \max_{0\le\omega\le\infty} |S(j\omega)| = \max_{0\le\omega\le\infty} \left|\frac{1}{1 + G(j\omega)C(j\omega)}\right| \quad (36)$$

where $G(s)$ and C(s) denote the plant and controller's transfer functions in s-domain for a unity negative feedback control system. Sensitivity and complementary sensitivity functions always and at all frequencies equals 1 for single-input and single-output systems. Accordingly, nominal complementary sensitivity peak of a system is given as:

$$M_{cs} = \max_{0\le\omega\le\infty} |S(j\omega)| = \max_{0\le\omega\le\infty} \left|\frac{G(j\omega)C(j\omega)}{1 + G(j\omega)C(j\omega)}\right| \quad (37)$$

The M_s is closely associated with the robustness of a system as it represents the inverse of the shortest distance from the Nyquist Curve of the loop-transfer function to the critical point -1. The further the loop-transfer function from the critical point in the complex plane the more robust the system is and the more it can handle unmodeled dynamics in the plant. Figure 30 indicates the M_s and M_{cs} values of the proposed PR-P current controlled inverter in dB.

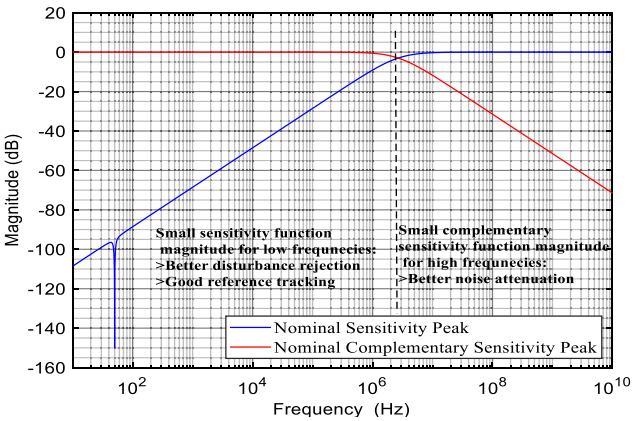

FIGURE 30. Robustness analysis of the system in terms of sensitivity and complementary sensitivity functions.

In addition to have small M_s in low frequencies and small M_{cs} for high frequencies, the peaks at the crossover point of these quantities are not desirable. For satisfactory control systems, the peak value of M_s must be in the range of 1.2-2 and the peak value of M_{cs} must be in the range of 1-1.5. Regarding this, the proposed system demonstrates very smooth roll-off at the crossover point of the curves.

V. CONCLUSION

This paper has presented an alternative unprecedented design process for a Proportional-Resonant (PR) controller with a selective harmonic components (3rd and 5th order) compensator for Photovoltaic Emulator (PVE) supported single phase Grid Connected Inverter (GCI) systems. The design procedure of the proposed controller unity proportional resonant (PR) path is conducted based on notch filter dynamics regulated by symmetrical pole placement methods. Addition of scheduled proportional gain designed

by loop shaping method to the resonant path increased the performance of the controller in terms of robustness, achieving better results in the presence of non-linear load and weak grid. The performance of the proposed controller and harmonic compensator is validated employing a PVE consisting of a DC-DC Buck converter, a Maximum Power Point Tracking (MPPT) algorithm and a full-bridge GCI designed using MATLAB/Simulink platforms. Frequency and time domain analysis of the system elements showed satisfactory behaviors. A comparative analysis with different PR controller design techniques used in various papers is performed and resulted in confirming that the proposed technique is robust and simple to implement. The performance of the Proposed PR-P controller with the harmonic compensator is compared with a PI in stationary reference frame and conventional PR current controllers in terms of steady-state error and harmonics mitigation. The simulation results demonstrated that the proposed PR-P controller with harmonic compensator is superior at tracking sinusoidal reference current with zero steady-state error and lower total harmonic distortion with eliminated 3rd and 5th order harmonics. The overall system is under development and experimental results will be presented in the near future.

COMPETING INTERESTS

The authors declare that they have no competing interests.

REFERENCES

[1] R. Ayop and C. W. Tan, "A comprehensive review on photovoltaic emulator," *Renew. Sustain. Energy Rev.*, vol. 80, pp. 430–452, Dec. 2017.
[2] S. Seyam, I. Dincer, and M. Agelin-Chaab, "Development of a clean power plant integrated with a solar farm for a sustainable community," *Energy Convers. Manage.*, vol. 225, Dec. 2020, Art. no. 113434.
[3] W. Xiao, *Photovoltaic Power Systems: Modeling, Design, and Control*, 1st ed. Hoboken, NJ, USA: Wiley, 2017.
[4] G. Price, *Renewable Power and Energy*, 1st ed. New York, NY, USA: Momentum Press, 2018.
[5] B. Carrera and K. Kim, "Comparison analysis of machine learning techniques for photovoltaic prediction using weather sensor data," *Sensors*, vol. 20, no. 11, p. 3129, Jun. 2020.
[6] L.-L. Li, S.-Y. Wen, M.-L. Tseng, and C.-S. Wang, "Renewable energy prediction: A novel short-term prediction model of photovoltaic output power," *J. Cleaner Prod.*, vol. 228, pp. 359–375, Aug. 2019.
[7] A. M. Padiyar and K. R. Kulkarni, *Dynamics and Control of Electric Transmission and Microgrids*, 1st ed. Hoboken, NJ, USA: Wiley, 2018.
[8] A. Sangwongwanich, Y. Yang, D. Sera, H. Soltani, and F. Blaabjerg, "Analysis and modeling of interharmonics from grid-connected photovoltaic systems," *IEEE Trans. Power Electron.*, vol. 33, no. 10, pp. 8353–8364, Oct. 2018.
[9] Y. Yang, K. Zhou, and F. Blaabjerg, "Current harmonics from single-phase grid-connected inverters—Examination and suppression," *IEEE J. Emerg. Sel. Topics Power Electron.*, vol. 4, no. 1, pp. 221–233, Mar. 2016.
[10] W. P. Mohan, N. Undeland, and T. M. Robbins, *Power Electronics: Converters, Applications, and Design*, 3rd ed. Hoboken, NJ, USA: Wiley, 2003.
[11] S.-H. Hwang and J.-M. Kim, "Dead time compensation method for voltage-fed PWM inverter," *IEEE Trans. Energy Convers.*, vol. 25, no. 1, pp. 1–10, Mar. 2010.
[12] *IEEE Standards Coordinating Committee 21 on Fuel Cells Photovoltaics Dispersed Generation and Energy Storage, IEEE Recommended Practice for Utility Interface of Photovoltaic (PV) Systems*, Standard, 2000.
[13] M. Shahabuddin, A. Riyaz, M. Asim, M. M. Shadab, A. Sarwar, and A. Anees, "Performance based analysis of solar PV emulators: A review," in *Proc. Int. Conf. Comput. Characterization Techn. Eng. Sci. (CCTES)*, Sep. 2018, pp. 94–99.
[14] I. Moussa and A. Khedher, "Photovoltaic emulator based on PV simulator RT implementation using XSG tools for an FPGA control: Theory and experimentation," *Int. Trans. Electr. Energy Syst.*, vol. 29, no. 8, pp. 1–16, Aug. 2019.
[15] I. Jayawardana, C. N. M. Ho, and M. Pokharel, "Design and implementation of switch-mode solar photovoltaic emulator using power-hardware-in-the-loop simulations for grid integration studies," in *Proc. IEEE Energy Convers. Congr. Exposit. (ECCE)*, Sep. 2019, pp. 889–894.
[16] S. Silwal and M. Karimi-Ghartemani, "On the design of proportional resonant controllers for single-phase grid-connected inverters," in *Proc. 12th IEEE Int. Conf. Control Automat. (ICCA)*, Jun. 2016, pp. 797–803.
[17] A. A. Nazeri, P. Zacharias, F. M. Ibanez, and S. Somkun, "Design of proportional-resonant controller with zero steady-state error for a single-phase grid-connected voltage source inverter with an LCL output filter," in *Proc. IEEE Milan PowerTech*, Jun. 2019, pp. 2–7.
[18] M. Parvez, M. F. M. Elias, and N. A. Rahim, "Performance analysis of PR current controller for single-phase inverters," in *Proc. 4th IET Clean Energy Technol. Conf. (CEAT)*, 2016, pp. 1–8.
[19] D. Zammit, C. S. Staines, M. Apap, and J. Licari, "Design of PR current control with selective harmonic compensators using MATLAB," *J. Electr. Syst. Inf. Technol.*, vol. 4, no. 3, pp. 347–358, Dec. 2017.
[20] H. Oruganti, S. Dash, C. Nallaperumal, and S. Ramasamy, "A proportional resonant controller for suppressing resonance in grid tied multilevel inverter," *Energies*, vol. 11, no. 5, p. 1024, Apr. 2018.
[21] E. N. Chaves, E. A. A. Coelho, G. P. Viajante, L. C. G. Freitas, L. G. Wezs, L. C. Freitas, C. A. Queiroz, and V. R. Bernadeli, "A control strategy design applied to single-phase grid-connected inverters," *Renew. Energy Power Qual.*, vol. 1, no. 14, pp. 731–735, May 2016.
[22] T.-K. Vu and S.-J. Seong, "Comparison of PI and PR controller based current control schemes for single-phase grid-connected PV inverter," *J. Korea Academia-Ind. Cooperation Soc.*, vol. 11, no. 8, pp. 2968–2974, Aug. 2010.
[23] T. Sathiyanarayanan and S. Mishra, "Synchronous reference frame theory based model predictive control for grid connected photovoltaic systems," *IFAC-PapersOnLine*, vol. 49, no. 1, pp. 766–771, 2016.
[24] R. S. Herrera, P. Salmerón, and H. Kim, "Instantaneous reactive power theory applied to active power filter compensation: Different approaches, assessment, and experimental results," *IEEE Trans. Ind. Electron.*, vol. 55, no. 1, pp. 184–196, Jan. 2008.
[25] C. Khomsi, M. Bouzid, K. Jelassi, and G. Champenois, "Harmonic current conpensation in a single-phase grid connected photovoltaic system sypplying nonlinear load," in *Proc. 9th Int. Renew. Energy Congr. (IREC)*, Mar. 2018, pp. 1–6.
[26] A. Kulkarni and V. John, "Mitigation of lower order harmonics in a grid-connected single-phase PV inverter," *IEEE Trans. Power Electron.*, vol. 28, no. 11, pp. 5024–5037, Nov. 2013.
[27] S. Pradhan, I. Hussain, B. Singh, and B. K. Panigrahi, "Performance improvement of grid-integrated solar PV system using DNLMS control algorithm," *IEEE Trans. Ind. Appl.*, vol. 55, no. 1, pp. 78–91, Jan./Feb. 2016.
[28] J. A. Suul, K. Ljøkelsøy, T. Midtsund, and T. Undeland, "Synchronous reference frame hysteresis current control for grid converter applications," *IEEE Trans. Ind. Appl.*, vol. 47, no. 5, pp. 2183–2194, Sep. 2011.
[29] U. Tamrakar, D. Shrestha, N. Malla, Z. Ni, T. Hansen, I. Tamrakar, and R. Tonkoski, "Comparative analysis of current control techniques to support virtual inertia applications," *Appl. Sci.*, vol. 8, no. 12, p. 2695, Dec. 2018.
[30] H. Mohomad, S. A. Saleh, and L. Chang, "Disturbance estimator-based predictive current controller for single-phase interconnected PV systems," *IEEE Trans. Ind. Appl.*, vol. 53, no. 5, pp. 4201–4209, Sep. 2017.
[31] M. A. R. Haider, S. A. Saleh, R. Shao, and L. Chang, "Robust current controller for grid-connected voltage source inverter," in *Proc. IEEE 8th Int. Symp. Power Electron. Distrib. Gener. Syst. (PEDG)*, Apr. 2017, pp. 1–7.
[32] F. Blaabjerg, R. Teodorescu, M. Liserre, and A. V. Timbus, "Overview of control and grid synchronization for distributed power generation systems," *IEEE Trans. Ind. Electron.*, vol. 53, no. 5, pp. 1398–1409, Oct. 2006.
[33] M. Ciobotaru, R. Teodorescu, and F. Blaabjerg, "Control of single-stage single-phase PV inverter," *EPE J.*, vol. 16, no. 3, pp. 20–26, Sep. 2006.
[34] Y. Du and D. D. C. Lu, "Harmonic distortion caused by single-phase grid-connected PV inverter," in *Power System Harmonics: Analysis, Effects and Mitigation Solutions for Power Quality Improvement*, A. Zobaa, S. H. E. A. Aleem, and M. E. Balci, Eds. 2018, pp. 51–63.

[35] M. Castilla, J. Miret, J. Matas, L. G. de Vicuña, and J. M. Guerrero, "Control design guidelines for single-phase grid-connected photovoltaic inverters with damped resonant harmonic compensators," *IEEE Trans. Ind. Electron.*, vol. 56, no. 11, pp. 4492–4501, Nov. 2009.
[36] S. Bacha, I. Munteanu, and A. I. Bratcu, *Power Electronic Converters Modeling and Control: With Case Studies* (Advanced Textbooks in Control and Signal Processing). London, U.K.: Springer, 2014.
[37] S. Silwal, S. Taghizadeh, M. Karimi-Ghartemani, M. J. Hossain, and M. Davari, "An enhanced control system for single-phase inverters interfaced with weak and distorted grids," *IEEE Trans. Power Electron.*, vol. 34, no. 12, pp. 12538–12551, Dec. 2019.
[38] T. D. C. Busarello, J. A. Pomilio, and M. G. Simoes, "Design procedure for a digital proportional-resonant current controller in a grid connected inverter," in *Proc. IEEE 4th Southern Power Electron. Conf. (SPEC)*, Dec. 2018, pp. 1–8.
[39] R. B. Bollipo, S. Mikkili, and P. K. Bonthagorla, "Critical review on PV MPPT techniques: Classical, intelligent and optimisation," *IET Renew. Power Gener.*, vol. 14, no. 9, pp. 1433–1452, Jul. 2020.
[40] G. Bayrak and D. Ghaderi, "An improved step-up converter with a developed real-time fuzzy-based MPPT controller for PV-based residential applications," *Int. Trans. Electr. Energy Syst.*, vol. 29, no. 12, pp. 1–20, Dec. 2019.
[41] A. Ba, C. O. Ehssein, M. E. M. O. M. Mahmoud, O. Hamdoun, and A. Elhassen, "Comparative study of different DC/DC power converter for optimal PV system using MPPT (P&O) method," *Appl. Sol. Energy*, vol. 54, no. 4, pp. 235–245, Jul. 2018.
[42] M. A. Ghasemi, A. Ramyar, and H. Iman-Eini, "MPPT method for PV systems under partially shaded conditions by approximating I–V curve," *IEEE Trans. Ind. Electron.*, vol. 65, no. 5, pp. 3966–3975, May 2018.
[43] A. Lashab, D. Sera, and J. M. Guerrero, "A dual-discrete model predictive control-based MPPT for PV systems," *IEEE Trans. Power Electron.*, vol. 34, no. 10, pp. 9686–9697, Oct. 2019.
[44] A. Amir, A. Amir, J. Selvaraj, N. A. Rahim, and A. M. Abusorrah, "Conventional and modified MPPT techniques with direct control and dual scaled adaptive step-size," *Sol. Energy*, vol. 157, pp. 1017–1031, Nov. 2017.
[45] R. González-Medina, I. Patrao, G. Garcerá, and E. Figueres, "A low-cost photovoltaic emulator for static and dynamic evaluation of photovoltaic power converters and facilities," *Prog. Photovolt., Res. Appl.*, vol. 22, no. 2, pp. 227–241, Feb. 2014.
[46] S. M. Azharuddin, M. Vysakh, H. V. Thakur, B. Nishant, T. S. Babu, K. Muralidhar, D. Paul, B. Jacob, K. Balasubramanian, and N. Rajasekar, "A near accurate solar PV emulator using dSPACE controller for real-time control," *Energy Procedia*, vol. 61, pp. 2640–2648, Jan. 2014.
[47] R. Ayop and C. W. Tan, "A novel photovoltaic emulator based on current-resistor model using binary search computation," *Sol. Energy*, vol. 160, pp. 186–199, Jan. 2018.
[48] J. P. Ram, H. Manghani, D. S. Pillai, T. S. Babu, M. Miyatake, and N. Rajasekar, "Analysis on solar PV emulators: A review," *Renew. Sustain. Energy Rev.*, vol. 81, pp. 149–160, Jan. 2018.
[49] H. Patel and V. Agarwal, "MATLAB-based modeling to study the effects of partial shading on PV array characteristics," *IEEE Trans. Energy Convers.*, vol. 23, no. 1, pp. 302–310, Mar. 2008.
[50] I. Moussa, A. Khedher, and A. Bouallegue, "Design of a low-cost PV emulator applied for PVECS," *Electronics*, vol. 8, no. 2, p. 232, Feb. 2019.
[51] P. Motsoeneng, J. Bamukunde, and S. Chowdhury, "Comparison of perturb & observe and Hill climbing MPPT schemes for PV plant under cloud cover and varying load," in *Proc. IREC*, 2019, pp. 1–6.

CAGFER YANARATES was born in April 1986. He received the M.Sc. degree in power engineering and sustainable energy FHEQ7 Taught master's/P.G.Dip./P.G.Cert. from Swansea University, in 2017, where he is currently pursuing the Ph.D. degree with the Electrical and Electronic Engineering Department. His research interest includes applications of power electronics converters in photovoltaics systems and their control.

ZHONGFU ZHOU received the Ph.D. degree from the University of Sussex, Brighton, U.K., in 2004. He joined the College of Engineering, Swansea University, in 2004, as a Research Officer and was promoted to a Lecturer in power electronics, in July 2016. His research interests include active rectifier, active power filter, and power electronics applications for renewable energy systems and automotive. Since 2010, he has been a member of the International Electrotechnical Commission (IEC), where he has advised on the internal standard (IEC TS 62600-30) on electrical power quality requirements for wave, tidal, and other water current energy converters.